



City Research Online

## City, University of London Institutional Repository

---

**Citation:** Kewlani, G., Vogiatzaki, K., Shanbhogue, S. & Ghoniem, A. F. (2013). Validation study of large-eddy simulations of wake stabilized reacting flows using artificial flame thickening approaches. 51st AIAA Aerospace Sciences Meeting including the New Horizons Forum and Aerospace Exposition 2013, doi: 10.2514/6.2013-169

This is the accepted version of the paper.

This version of the publication may differ from the final published version.

---

**Permanent repository link:** <https://openaccess.city.ac.uk/id/eprint/12318/>

**Link to published version:** <https://doi.org/10.2514/6.2013-169>

**Copyright:** City Research Online aims to make research outputs of City, University of London available to a wider audience. Copyright and Moral Rights remain with the author(s) and/or copyright holders. URLs from City Research Online may be freely distributed and linked to.

**Reuse:** Copies of full items can be used for personal research or study, educational, or not-for-profit purposes without prior permission or charge. Provided that the authors, title and full bibliographic details are credited, a hyperlink and/or URL is given for the original metadata page and the content is not changed in any way.

---

City Research Online:

<http://openaccess.city.ac.uk/>

[publications@city.ac.uk](mailto:publications@city.ac.uk)

---

# Validation Study of Large-Eddy Simulations of Wake Stabilized Reacting Flows using Artificial Flame Thickening Approaches

Gaurav Kewlani<sup>1</sup>, Konstantina Vogiatzaki<sup>2</sup>, Santosh Shanbhogue<sup>3</sup>, and Ahmed F. Ghoniem<sup>4</sup>  
*Massachusetts Institute of Technology, Cambridge, MA, 02139*

Wake flows are the preferred mode of flame stabilization in lean premixed combustion in gas turbine engines, low NOx burners, afterburners etc. These flows exhibit inherent unsteadiness and for their numerical modeling and simulations, large eddy simulation (LES) techniques with an appropriate combustion model and reaction mechanism afford a balance between computational complexity and predictive accuracy. Before using them in practical systems, these techniques must be validated against experimental measurements in a number of canonical cases. In this work, results from LES of non-reacting and reacting flows are compared to data from a number of experiments, corresponding to the following configurations: a triangular bluff body in a rectangular duct, a backward facing step, and a cylindrical sudden expansion with swirl. The artificial flame thickening approach is applied for modeling turbulence-combustion interactions at small scales. Algebraic and equation-based efficiency function models are implemented, along with an appropriate reduced chemistry mechanism. A novel dynamic formulation for the efficiency function based on the flame-wrinkling equation that explicitly incorporates the influence of strain and time-history effects is proposed, and a detailed combustion chemistry mechanism is also used. Results show that the approaches are effective in simulating turbulent premixed combustion.

## Nomenclature

|                      |   |                                |
|----------------------|---|--------------------------------|
| $s_L^0$              | = | unstrained laminar flame speed |
| $D$                  | = | molecular diffusivity          |
| $\bar{\omega}$       | = | mean reaction rate             |
| $\delta_L^0$         | = | laminar flame thickness        |
| $F$                  | = | thickening factor              |
| $E$                  | = | efficiency function            |
| $\rho$               | = | density                        |
| $Y_i$                | = | species mass fraction          |
| $\tilde{\mathbf{u}}$ | = | filtered velocity vector       |
| $\tilde{\omega}_i$   | = | filtered species reaction rate |
| $c$                  | = | reaction progress variable     |
| $Y_F^{in}$           | = | fuel mass fraction at inlet    |
| $F_{loc}$            | = | local thickening factor        |
| $D_{loc}$            | = | local diffusivity              |
| $\mu$                | = | dynamic viscosity              |
| $Sc$                 | = | Schmidt number                 |
| $\Xi$                | = | flame wrinkling factor         |
| $\Delta_c$           | = | local filter width             |

---

<sup>1</sup> Research Assistant, Department of Mechanical Engineering, Room 3-339.

<sup>2</sup> Post-Doctoral Associate, Department of Mechanical Engineering, Room 3-339.

<sup>3</sup> Research Scientist, Department of Mechanical Engineering, Room 3-339.

<sup>4</sup> Ronald C. Crane ('72) Professor, Department of Mechanical Engineering, 3-342, AIAA Member

|                 |   |  |
|-----------------|---|--|
| $Re_t$          | = | turbulent Reynold number                                   |
| $u'_{\Delta_e}$ | = | SGS turbulent velocity                                     |
| $n$             | = | normal to flame surface                                    |
| $b$             | = | reaction regress variable                                  |
| $U_s$           | = | local instantaneous velocity of the flame surface          |
| $U_t$           | = | surface-filtered effective velocity of the flame           |
| $\sigma_s$      | = | surface filtered resolved strain rate (relating to $U_s$ ) |
| $\sigma_t$      | = | resolved strain rate (relating to $U_t$ )                  |
| $\tau_\eta$     | = | Kolmogorov timescale                                       |
| $u'$            | = | sub-grid turbulence intensity                              |
| $R_\eta$        | = | Kolmogorov Reynolds number                                 |
| $\sigma_{ext}$  | = | extinction strain rate                                     |
| $s_u$           | = | strained laminar burning velocity                          |
| $Re_\Delta$     | = | SGS turbulent Reynolds number                              |

## I. Introduction

Lean premixed combustion is a promising technology for many industrial-scale applications such as gas turbine systems, primarily because of its benefits such as low pollutant emissions. A drawback of premixed combustion, however, is that it is prone to thermo-acoustic instability. Recirculating flows in the wake of a bluff-body, behind a sudden expansion or downstream a swirler, are often used to anchor the flame and to expand the stability range. Understanding turbulent combustion mechanisms in such configurations has been challenging and remains an active area of research in the combustion community [1]. The purpose of these studies is to develop a fundamental understanding of combustion dynamics and flame stability, as well as to assess the performance in terms of power density, efficiency and emissions. Numerical modeling and simulations are increasingly being used to predict the performance of such systems, as the approach is more flexible and cost effective as compared to a detailed experimental investigation.

Large-Eddy Simulations (LES) with appropriate turbulent combustion models and reaction mechanisms are considered as one of the more promising approaches, balancing computational complexity and predictive accuracy. While Direct Numerical Simulations (DNS) resolve all the turbulent scales, they are computationally expensive and impractical for high Reynolds number large scale applications. Solving the Reynolds Averaged Navier Stokes Equations (RANS), on the other hand, models the influence of turbulence on the mean flow and hence can not capture the unsteady flow. In LES, rather than averaging the effect of turbulence, the equations are filtered, enabling the larger scales of turbulence to be explicitly resolved, while the effect of the smallest ones on the large scales is modeled. The governing equations are obtained by applying the Favre filtering operation to each term in the instantaneous conservation equations of mass, momentum and energy, and the species transport equations [2]. This enables capturing part of the inherent flow unsteadiness in the flow, which is particularly important when dynamics at the large scales play an important role. Modeling the sub-grid scale effects on the other hand ensures that the approach is computationally manageable.

An important component of LES is the turbulent combustion sub-grid model, which is necessary to incorporate the effect of turbulence-chemistry interactions at the unresolved scales on the reaction rate. Various approaches have been developed, such as eddy break-up type models, flame surface density and flame wrinkling descriptions, the level-set flame front tracking technique (G-equation approach), and the artificially thickened flame technique [3]. Evaluating the performance of these sub-models is crucial to developing higher fidelity CFD methods for predicting combustion dynamics.

LES validation studies have been conducted in the past [4-7] using the thickened flame approaches to assess their predictive capabilities in turbulent combustion. In most of these numerical simulations, the calculations of the reaction rate in the combustion models have used fairly simple reaction chemistry (1-2 reaction steps). More detailed schemes need to be incorporated within the existing framework to predict flame temperatures more accurately. Moreover, further development of the model is warranted so that the approach can be applied to the analysis of strongly unsteady systems [6].

This work addresses some of these concerns, by incorporating a dynamic formulation for the efficiency function, based on the solution of a transport equation for flame wrinkling [8] that results in accurate predictions for highly unsteady combustion systems, especially those prone to thermo-acoustic instability. Detailed reaction chemistry that can be appropriately used with the thickened flame approach [9] is also included.

In this study, numerical simulations are performed using a compressible LES code for unsteady lean premixed combustion in the following configurations: triangular bluff body in a rectangular duct, a backward facing step, and a cylindrical sudden expansion with swirl, providing a reasonably comprehensive framework for the validation of the combustion model.

As mentioned above, for modeling turbulent combustion, the thickened flame approach is implemented, and the performance of different efficiency function models is studied. The effect of reaction chemistry on the predictions is also investigated. Section II provides a brief description of the combustion models employed in this study. In Section III, the experimental configuration and the simulation setups are described. The results are subsequently discussed in Section IV, and the conclusions are presented in Section V.

## II. Turbulent Combustion Modeling

Modeling of the filtered reaction rates presents a major challenge in turbulent premixed combustion. This is because reaction rates are highly nonlinear functions of temperature and species mass fractions, and because chemical reactions are confined to thin reacting layers at small scales that cannot be resolved on typical LES grids. As a consequence, turbulence-chemistry interaction needs to be modeled. A number of combustion models and approaches have been suggested for LES of turbulent combustion. In this work, the focus is on the artificially thickened flame approach. In this section, a brief description of the method, as implemented in this study, is presented.

The thickened flame (TF) approach essentially involves artificial thickening of the flame-front so that it can be resolved on the LES grid, while maintaining the same laminar flame speed and turbulence-flame interaction. From the theory of laminar premixed flames, it is known that the laminar flame speed,  $s_L^0$ , and the laminar flame thickness,  $\delta_L^0$ , are related to the molecular diffusivity ( $D$ ) and the mean reaction rate ( $\bar{\omega}$ ) as follows:

$$s_L^0 \propto \sqrt{D\bar{\omega}}, \delta_L^0 \propto D/s_L^0 = \sqrt{D/\bar{\omega}} \quad (1),(2)$$

Increasing the flame thickness by a factor  $F$  while maintaining a constant flame speed can be achieved by suitably modifying the diffusivity and the mean reaction rate (by replacing  $D$  with  $FD$ , and  $\bar{\omega}$  with  $\bar{\omega}/F$ ). If  $F$  is sufficiently large, the thickened flame front can be resolved on the LES computational grid. The thickening of the flame front, however, leads to a modified interaction between turbulence and chemistry since the Damkohler number is decreased by the factor  $F$ . The flame becomes less sensitive to turbulence, and wrinkling of the flame front is reduced. To account for this, an efficiency function,  $E$ , is introduced [4] that recovers the underestimation of the flame front wrinkling by the approach. The balance equation for the chemical species then takes the form:

$$\frac{\partial \bar{\rho} \tilde{Y}_i}{\partial t} + \frac{\partial (\bar{\rho} \tilde{Y}_i \tilde{u}_j)}{\partial x_j} = \frac{\partial}{\partial x_j} \left( \bar{\rho} E F D_i \frac{\partial \tilde{Y}_i}{\partial x_j} \right) + \frac{E \bar{\omega}_i}{F} \quad (3)$$

where  $\rho$  is the density,  $Y_i$  is species mass fraction,  $\tilde{\mathbf{u}}$  is the filtered velocity vector, and  $\bar{\omega}_i$  is the filtered species reaction rate.

It may be noted, however, that the above approach modifies the diffusion term in the whole domain, which can lead to inaccuracies in the prediction of the species mass fractions. To overcome this, a dynamic formulation has been proposed [10], wherein the thickening factor and the diffusivity are represented locally as follows:

$$F_{loc} = 1 + (F - 1) \Psi(c), \quad D_{i,loc} = \frac{\mu}{Sc} E F_{loc} + (1 - \Psi(c)) \frac{\mu_i}{Sc_i} \quad (4),(5)$$

$$\Psi(c) = 16[c(1-c)]^2, \quad c = 1 - Y_F / Y_F^{in} \quad (6),(7)$$

where,  $\Psi(c)$  is a locally defined function based on the reaction progress variable,  $c$ , prescribed in terms of the ratio of the fuel mass fraction in the cell ( $Y_F$ ) to that at the inlet ( $Y_F^{in}$ ). The symbols  $\mu$  and  $Sc$  refer to the dynamic viscosity and the Schmidt number respectively, while  $F_{loc}$  and  $D_{i,loc}$  refer to the local thickening factor and local diffusivity respectively. The species transport equation can then be rewritten as follows:

$$\frac{\partial \bar{\rho} \tilde{Y}_i}{\partial t} + \frac{\partial (\bar{\rho} \tilde{Y}_i \tilde{u}_j)}{\partial x_j} = \frac{\partial}{\partial x_j} \left( \bar{\rho} E F_{loc} D_{i,loc} \frac{\partial \tilde{Y}_i}{\partial x_j} \right) + \frac{E \bar{\omega}_i}{F_{loc}} \quad (8)$$

An important aspect of the thickened flame approach is the evaluation of the efficiency function  $E$ , in order to appropriately account for the reduced wrinkling of the thickened flame front due to turbulence. Based on DNS studies of flame-vortex interactions [5], different models have been proposed to define  $E$  in terms of the dimensionless wrinkling factor  $\Xi$ , which can be treated as the ratio of flame surface to its projection in the direction of propagation.

Colin et al. [5] suggested the following expression for modeling the efficiency function in terms of the local filter width,  $\Delta_e$ , the unstrained laminar flame speed,  $s_L^0$ , the thickness of the laminar ( $\delta_L^0$ ) and thickened flames ( $\delta_L^1$ ), and the local SGS turbulent velocity,  $u'_{\Delta_e}$ :

$$E = \frac{\Xi|_{\delta_L=\delta_L^0}}{\Xi|_{\delta_L=\delta_L^1}} \geq 1 \quad (9)$$

$$\Xi = 1 + \alpha \left( \frac{2 \ln 2}{3C_{ms}(\text{Re}_t^{1/2} - 1)} \right) \frac{u'_{\Delta_e}}{s_L^0} \Gamma \left( \frac{\Delta_e}{\delta_L^0}, \frac{u'_{\Delta_e}}{s_L^0} \right) \quad (10)$$

$$\Gamma \left( \frac{\Delta_e}{\delta_L^0}, \frac{u'_{\Delta_e}}{s_L^0} \right) = 0.75 \exp \left[ -1.2 \left( \frac{u'_{\Delta_e}}{s_L^0} \right)^{-0.3} \right] \left( \frac{\Delta_e}{\delta_L^0} \right)^{2/3} \quad (11)$$

where  $\text{Re}_t$  is the turbulent Reynolds number, and  $\alpha$ ,  $C_{ms}$  are model constants ( $\alpha = 1$ ,  $C_{ms} = 0.28$ ).

A possible limitation of the approach, as highlighted in [6], is that under highly unsteady conditions, the model can result in inaccurate predictions, since it assumes local equilibrium between production and destruction of SGS flame surface density. In this regard, a transport equation for the sub-grid flame wrinkling can be used to dynamically evaluate the magnitude of the efficiency function, by appropriately determining the model parameter  $\alpha$  during the LES computations. This equation can be written as [8]:

$$\frac{\partial \Xi}{\partial t} + \widehat{U} \cdot \nabla \Xi = -\widehat{n} \cdot (\nabla U_s) \cdot \widehat{n} \Xi + \widehat{n} \cdot (\nabla \widehat{U}_t) \cdot \widehat{n} \Xi + (\widehat{U}_t - \widehat{U}_s) \cdot \frac{\nabla |\nabla b|}{|\nabla b|} \Xi \quad (12)$$

where  $U_t$  is the surface-filtered effective velocity of the flame,  $U_s$  is the local instantaneous velocity of the flame surface,  $n$  is the normal to the flame surface, and  $b$  is the reaction regress variable. The terms on the right-hand side represent the effects of strain, propagation and differential propagation respectively. A simplified equation to (12) has been obtained by Weller [8] as:

$$\frac{\partial \Xi}{\partial t} + \widehat{U}_s \cdot \nabla \Xi = G \Xi - R(\Xi - 1) + (\sigma_s - \sigma_t) \Xi \quad (13)$$

$$G = R \frac{2c(\Xi_{eq}^* - 1)}{1 + 2c(\Xi_{eq}^* - 1)}, R = \frac{0.28}{\tau_\eta} \frac{\Xi_{eq}^*}{\Xi_{eq}^* - 1}, \Xi_{eq}^* = 1 + 0.62 \sqrt{\frac{u'}{s_u}} R_\eta \quad (14)$$

where  $\tau_\eta$  is the Kolmogorov timescale,  $u'$  is the sub-grid turbulence intensity,  $c$  is the reaction progress variable and  $R_\eta$  is the Kolmogorov Reynolds number. The terms  $\sigma_s$  and  $\sigma_t$  refer to the resolved strain rate and the surface filtered resolved strain rate respectively, while  $s_u$  refers to the strained laminar burning velocity, and can be obtained as:

$$\frac{\partial s_u}{\partial t} + \widehat{U}_s \cdot \nabla s_u = -\sigma_s s_u + \sigma_s s_u^\infty \frac{(s_L^0 - s_u)}{(s_u - s_u^\infty)}, s_u^\infty = s_L^0 \max(1 - \sigma_s / \sigma_{ext}, 0) \quad (15)$$

where  $s_L^0$  is the unstrained laminar flame speed and  $\sigma_{ext}$  is the strain rate at extinction. Additional details on the modeling can be found in [8].

Once the value of the flame wrinkling is obtained using the above formulation, it can be used to estimate the model parameter  $\alpha$  from the wrinkling factor equation corresponding to the thickened flame (10). The model parameter and efficiency function magnitudes can therefore be dynamically evaluated during the computations.

In addition to updating the model parameter  $\alpha$ , the strained flame speed, as determined in (15), can also be used to replace the unstrained value in (11). This has been shown to have a significant effect on the predictions [11], and has therefore been incorporated in the current work. Another alternative to estimating the strained flame speed is to use empirical relations obtained using flamelet generated look-up tables as proposed in [11].

It should be noted that other models have also been proposed to estimate the efficiency function, such as the power-law model by Charlette et al. [6],[7]. This approach defines the efficiency function in terms of the local filter width  $\Delta_e$ , the laminar flame speed  $s_L^0$ , the laminar flame thickness  $\delta_L^0$ , the local SGS turbulent velocity  $u'_{\Delta_e}$  as:

$$E = \left( 1 + \min \left[ \frac{\Delta_e}{\delta_L^0}, \Gamma \frac{u'_{\Delta_e}}{s_L^0} \right] \right)^\alpha \quad (16)$$

$$\Gamma \left( \frac{\Delta_e}{\delta_L^0}, \frac{u'_{\Delta_e}}{s_L^0}, \text{Re}_\Delta \right) = [((f_u^{-a}) + (f_\Delta^{-a})^{-1/a})^{-b} + f_{\text{Re}}^{-b}]^{-1/b} \quad (17)$$

$$f_u = 4 \left( \frac{27C_k}{110} \right)^{1/2} \left( \frac{18C_k}{55} \right) \left( \frac{u'_{\Delta_e}}{s_L^0} \right)^2, f_\Delta = \left[ \frac{27C_k \pi^{4/3}}{110} \left( \left( \frac{\Delta_e}{\delta_L^0} \right)^{4/3} - 1 \right) \right]^{1/2}, f_{\text{Re}} = \left[ \frac{9}{55 \text{Re}_\Delta} \exp \left( -\frac{3}{2} C_k \pi^{4/3} \text{Re}_\Delta^{-1} \right) \right]^{1/2} \quad (18-20)$$

$$a = 0.6 + 0.2 \exp \left[ -0.1 \left( \frac{u'_{\Delta_e}}{s_L^0} \right) \right] - 0.20 \exp \left[ -0.01 \left( \frac{\Delta_e}{\delta_L^0} \right) \right], \Delta_e = F \delta_L^0, \text{Re}_\Delta = 4 \frac{\Delta_e u'_{\Delta_e}}{\delta_L^0 s_L^0} \quad (21-23)$$

where  $\text{Re}_\Delta$  is the SGS turbulent Reynolds number,  $\alpha$ ,  $b$  and  $C_k$  are model constants ( $\alpha = 0.5$ ,  $b = 1.4$ ,  $C_k = 1.5$ ).

A distinct advantage of the thickened flame approaches discussed above is that the reaction rates can be calculated using Arrhenius rate laws, much like a direct numerical simulation (DNS) calculation, without the need of any ad hoc sub-models, while allowing the explicit use of multi-step chemistry mechanisms as well. Moreover, phenomena such as ignition and flame-wall interactions are directly accounted for, without requiring additional sub-modeling.

In addition to the above, the proposed wrinkling based approach is an improvement over the existing algebraic models, since deviation from local equilibrium, and the absence of time history and strain effects in the equilibrium models can result in inaccurate predictions, especially in case of lean premixed flames under highly unsteady conditions.

In this work, the different efficiency function models described above have been implemented, along with appropriate chemistry mechanisms for methane/propane combustion in air, as indicated below:

- 1) Single-step chemistry with 5 species ( $\text{CH}_4/\text{C}_3\text{H}_8$ ,  $\text{O}_2$ ,  $\text{N}_2$ ,  $\text{CO}_2$ ,  $\text{H}_2\text{O}$ ) suggested by Westbrook-Dryer (WD) [12].
- 2) Reduced reaction chemistry with 5 reactions and 7 species, suggested by Jones-Lindstedt (JL) [13].

A multiple-step combustion chemistry mechanism is implemented to study the effect of the reaction chemistry on the predictions. While simplified global schemes can provide adequate results if the main species concentrations are of interest, they cannot be expected to work as well under unconventional combustion (e.g. oxy-fuel combustion conditions), and are likely to over-estimate the temperature in the absence of endothermic reactions. Moreover, the role of reaction chemistry can be significant in combustion systems prone to thermo-acoustic instabilities. It should be noted, however, that the reaction schemes used should typically include a limited number of intermediate species as it can lead to difficulties for wrinkled and/or stretched flame fronts [4][9].

### III. Experimental Configuration & Simulation Setup

The following canonical configurations are studied: triangular bluff body in a rectangular channel [12, 14], backward facing step [15], and cylindrical sudden expansion with swirl [16], and are chosen since they comprise many aspects of practical combustors such as anchored flames, regions of recirculation and shear layers. A parallelized, unstructured, finite volume LES code for solving compressible 3D Navier Stokes equations with second order spatial and temporal accuracy is used, and the one-equation eddy viscosity model is employed to estimate the SGS stresses for each case.

LES predictions are validated against experimental data for non-reacting and reacting cases. For each configuration, coarse and fine grids are utilized to ascertain the sensitivity of results to grid resolution, and the performance of different efficiency function models is also evaluated.

### A. Triangular Bluff Body in a Rectangular Channel

The bluff body configuration [12, 14] consists of a straight channel 600 mm long and a rectangular cross section of 120 mm  $\times$  240 mm. The flame is anchored on a bluff body that has a triangular cross section (each side,  $h = 40$  mm), located 500 mm upstream of the exit. A mixture of air and propane is introduced at an equivalence ratio of 0.65, at a bulk inlet velocity of 17.0 m/s ( $Re = 48,000$ ). The inlet temperature is 288 K and the nominal pressure is 101 kPa.

The non-uniform meshes (fine and coarse) comprise of 0.74 million and 0.37 million hexahedral cells respectively, and get coarser along the stream-wise direction. The numbers of cells in the x and y directions for the fine mesh are 525 and 140 respectively, while the corresponding numbers for the coarse mesh are 525 and 70 respectively.  $\Delta y$  for the fine and coarse mesh is 0.67mm and 1.33mm respectively in the wake region (1mm and 2mm respectively otherwise), while  $\Delta x$  for either mesh is 0.67mm immediately downstream of the bluff body (up to 100mm) and 1.33mm, on an average, thereafter.

Simulations over a sixth of the burner width with periodic boundary conditions in the span-wise direction are performed. At the inlet, Dirichlet conditions are used for all variables except the pressure, for which zero Neumann conditions are specified. The inlet velocity has a flat profile on which turbulent fluctuations are imposed. At the exit, zero Neumann conditions are specified for all variables except the pressure, for which wave-transmissive conditions are used. No-slip conditions are applied for the flow at the top and bottom walls of the duct as well as the bluff body, while zero Neumann conditions are specified for the other variables.

Simulations start from quiescent conditions and the unsteady flow characteristics evolve naturally. The time step is 10  $\mu s$  for the non-reacting flow and 2  $\mu s$  for the reacting case, and averaging is performed over nearly 11 flow-through cycles once the flow is established in the computational domain.

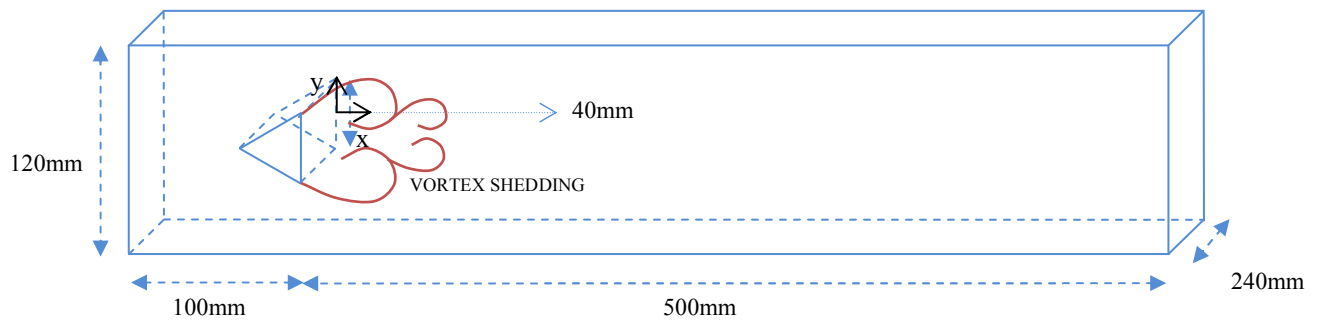


Figure 1: Bluff body setup used for flame stabilization.

### B. Backward Facing Step

The backward facing step configuration [15] consists of a step of height 25.4 mm and a rectangular cross section of 50.8 mm  $\times$  38.1 mm downstream of the step. A mixture of air and propane is introduced at an equivalence ratio of 0.6, at a bulk inlet velocity of 13.3 m/s ( $Re = 22,100$ ). The inlet temperature is 293 K and the nominal pressure is 101 kPa.

The non-uniform meshes (fine and coarse) comprise of 0.52 million and 0.26 million hexahedral cells respectively, and get coarser along the stream-wise direction. The numbers of cells in the x and y directions, downstream of the step, for the fine mesh are 393 and 120 respectively, while the corresponding numbers for the coarse mesh are 248 and 100 respectively. The average  $\Delta x$  downstream of the step is 0.67mm and 1mm for the fine and coarse mesh respectively.

Simulations over the entire burner width with periodic boundary conditions in the span-wise direction are performed. At the inlet, Dirichlet conditions are used for all variables except the pressure, for which zero Neumann conditions are specified. The inlet velocity has a flat profile on which turbulent fluctuations are imposed. At the exit, zero Neumann conditions are specified for all variables except the pressure, for which wave-transmissive conditions are used. No-slip conditions are applied for the flow at the top and bottom walls of the duct as well as the bluff body, while zero Neumann conditions are specified for the other variables (Note that heat transfer is also considered at the top and bottom walls).

Simulations start from quiescent conditions and the unsteady flow characteristics evolve naturally. The time step is 10  $\mu s$  for the non-reacting flow and 2  $\mu s$  for the reacting case, and averaging is performed over nearly 22 flow-through cycles once the flow is established in the computational domain.

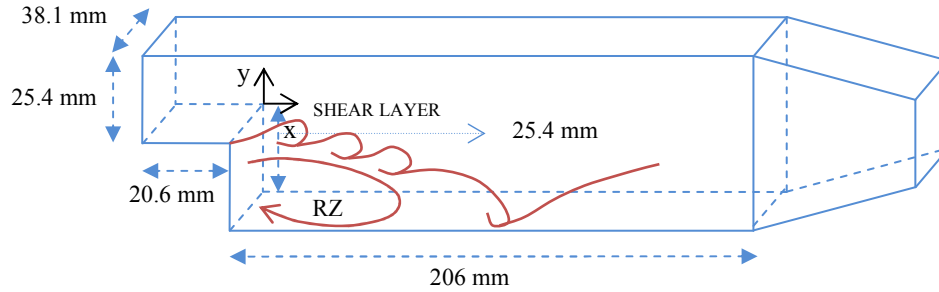


Figure 2: Backward facing step configuration used for flame stabilization.

### C. Cylindrical Sudden Expansion with Swirl

The cylindrical sudden expansion configuration [16], shown in figure 3, is designed to stabilize combustion using a combination of swirl and sudden expansion. A mixture of air and methane is introduced at an equivalence ratio of 0.66, through a 38 mm diameter pipe, at a bulk inlet velocity of 8.0 m/s ( $Re = 20,000$ ). The inlet temperature is 300 K and the nominal pressure is 101 kPa. The swirler, located 50 mm upstream of the expansion plane, has 8 blades each inclined at  $45^\circ$  to the cylinder cross-section, with an estimated swirl number of 0.7. More details on the experiment and measurement apparatus can be found in [17].

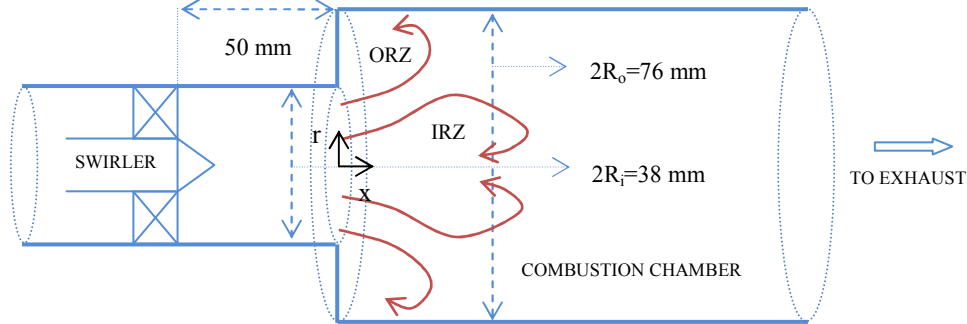


Figure 3. Swirler and cylindrical combustion chamber with dimensional details.

To provide an accurate comparison between numerical predictions and experimental measurements, the actual swirler geometry was meshed (figure 4) for the LES calculations, instead of imposing a swirling velocity profile at the inlet. This allows the simulated flow to evolve in a ‘realistic’ way as it passes through the blades.

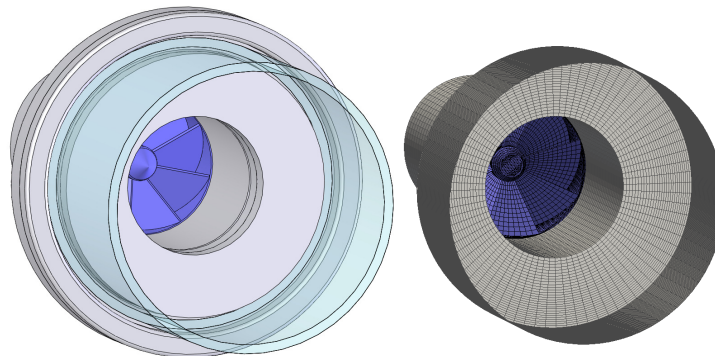


Figure 4. Swirl combustor geometry and corresponding mesh used in the analysis

The non-uniform meshes (fine and coarse) in the main combustion chamber downstream of the sudden expansion comprise of 0.34 million and 0.25 million hexahedral cells respectively, and get coarser along the stream-wise direction. The numbers of cells in the radial, tangential and axial directions corresponding to the fine mesh are 24, 80 and 175 respectively, with the average  $\Delta x$  and  $\Delta r$  as 1.2mm and 1.6mm respectively.

At the inlet, Dirichlet conditions are used for all variables except the pressure, for which zero Neumann conditions are specified. The inlet velocity has a flat profile on which turbulent fluctuations are imposed. At the exit, zero Neumann conditions are specified for all variables except the pressure, for which wave-transmissive conditions are used. No-slip conditions are applied for the flow at the top and bottom walls of the duct as well as the bluff body, while zero Neumann conditions are specified for the other variables (Note that heat transfer is also considered at the walls).

Simulations start from quiescent conditions and the unsteady flow characteristics evolve naturally. The time step is  $10 \mu\text{s}$  for the non-reacting flow and  $2 \mu\text{s}$  for the reacting case, and averaging is performed over nearly 10 flow-through cycles once the flow is established in the computational domain.

## IV. Results and Discussion

### A. Triangular Bluff Body: Non-Reacting Flow

Non-reacting flow is first simulated and the average and rms axial velocity profiles at different cross-sections across the length of the combustor are shown in figure 5, for the fine and the coarse meshes. It is observed that the flow is characterized by a strong recirculation zone in the immediate downstream region of the bluff body, featuring periodic asymmetric vortex shedding. Simulation results agree well with experimental measurements for both meshes and the underlying average flow field is suitably resolved in either case, though a slight discrepancy can be observed for the velocity fluctuation comparisons that could be attributed to the use of periodic boundary conditions.

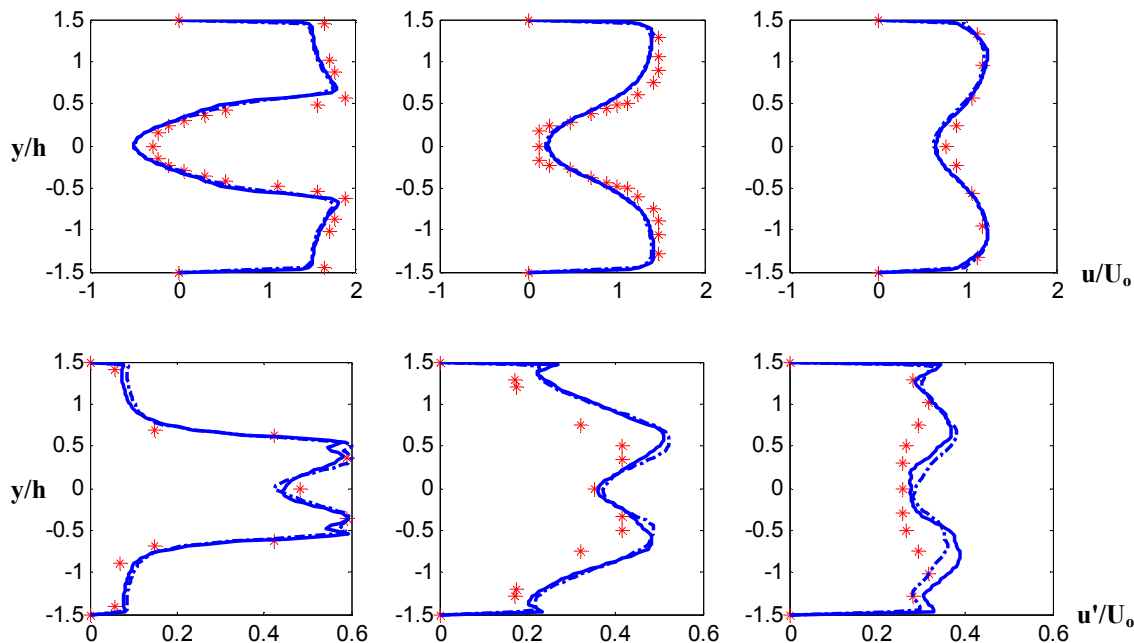


Figure 5: Normalized average/rms axial velocity profiles at  $x/h = 0.375, 1.5, 3.75$  (non-reacting flow):  
 \*\*\* Experiment, — LES (fine mesh), - - - LES (coarse mesh)

### B. Triangular Bluff Body: Reacting Flow

Next, reacting case validation is performed for the coarse mesh, using the different efficiency function models. A strong recirculation zone similar to the one present for the non-reacting case is noted for the reactive case, which however is longer and broader due to a more gradual dissipation of momentum in the wake region (figure 6). The flame anchors behind the bluff-body, primarily due to the recirculation of the combustion products in the wake region, and is essentially confined to a surface originating in the shear layers downstream of the flame-holder edges. Large scale mixing between the cold reactants and the hot products thus takes place in these shear layer regions, forming a composition in which combustion can occur (figure 8).

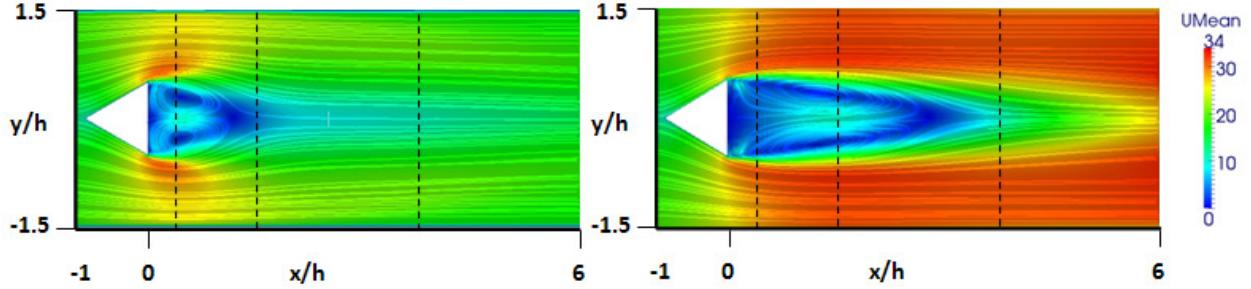


Figure 6: Average velocity magnitude contours and streamlines: non-reacting case (left), reacting case (right). The cross-sections at which data are compared are also shown.

The average and rms axial velocity profiles for the reacting case at different cross-sections across the length of the combustor are shown in figure 7. The simulation results corresponding to each of the combustion model reproduce the average flow field reasonably accurately, although the single step reaction mechanism results tend to deviate (essentially resulting from inaccurate, higher temperature estimation). It is also noted that the unsteadiness in the flow field as indicated by the rms profiles is better predicted using the dynamic formulation for the efficiency function, especially within the recirculation zone and shear layer regions. A higher peak reverse velocity is also observed as compared to the non-reactive case due to exothermicity.

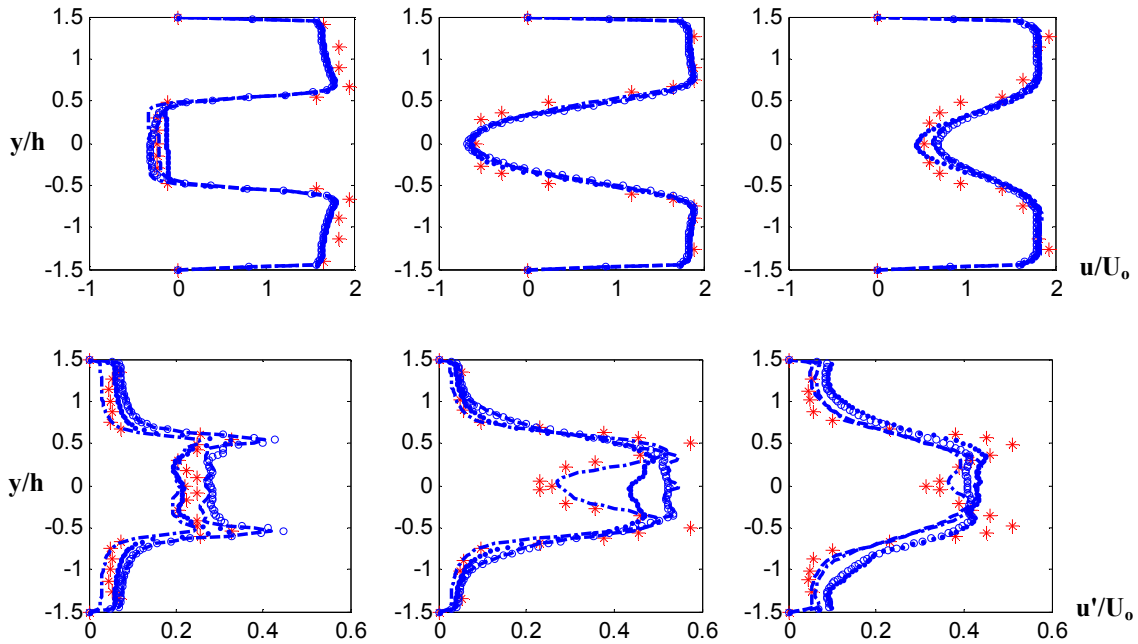


Figure 7: Normalized average/rms axial velocity profiles at  $x/h = 0.375, 1.5, 3.75$  (reacting flow, coarse grid):  
 \*\*\* Experiment, ●●● LES (Colin-Algebraic, WD), ○○○ LES (Colin-Algebraic, JL), - - - LES (Charlette, JL), - · - · LES (Colin-Dynamic, JL)

As pointed out earlier, the recirculation zone is responsible for anchoring the flame, as hot products are stored inside the wake, convected downstream and periodically mixed with the co-flowing fresh mixture by the shed vortices, while chemical reaction takes place in the shear layers between the wake and co-flowing fresh mixture.

It is also observed that as compared to the non-reacting case, the vorticity field is more diffuse, and the large-scale vortices are broken up directly after they have been formed, perhaps due to thermal expansion in the vortex cores. Further, the recirculation zone is characterized by periodic symmetric vortex shedding, as opposed to asymmetric vortex shedding in the non-reacting flow (figure 8). These vortices, periodically shed off the upper and lower edges of the bluff body, are responsible for the downstream convection and mixing of the hot products stored inside the wake with the fresh incoming mixture.

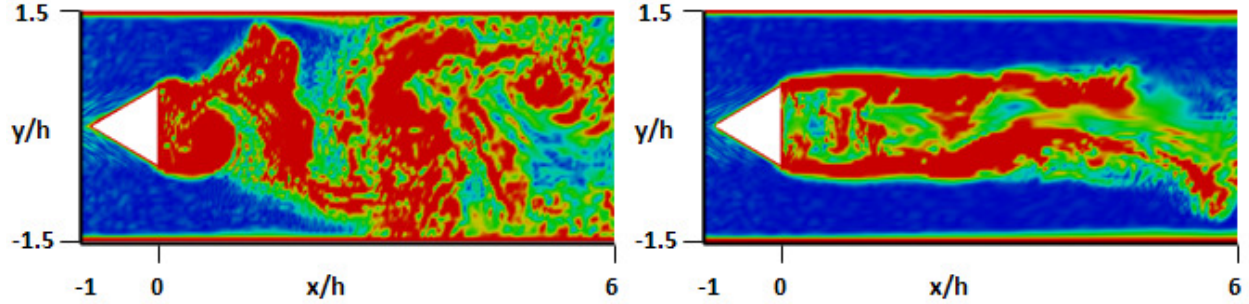


Figure 8: Instantaneous vorticity contours: non-reacting case (left) and reacting case (right).

The average temperature profiles for each of the cases are also compared with the experimental data (figure 9) and it is observed that the models tend to slightly under-predict the spreading rate of the flame, while the temperature is over-predicted, especially further downstream, when a global reaction mechanism is used (which likely over-estimates the temperature due to the absence of endothermic reactions). Similar predictions resulting in lower spread of the flame are obtained in [12] when periodic boundary conditions are used, and fully 3D simulations that can effectively capture the effects of all four walls (eg boundary layer thickening etc) may result in more accurate predictions for the temperature as well as velocity fluctuations.

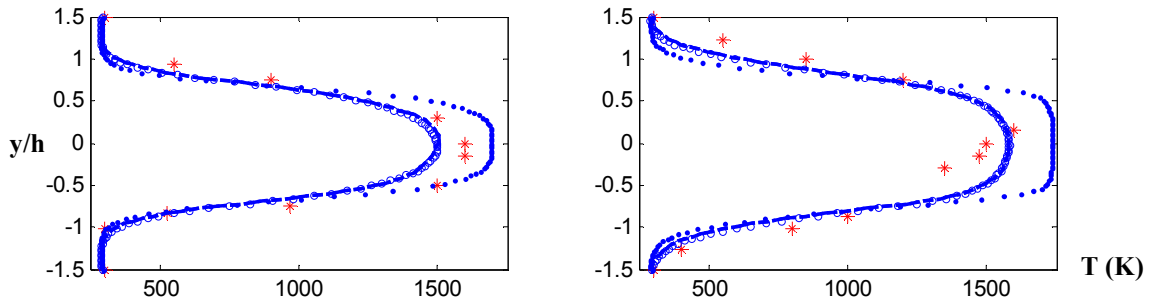


Figure 9: Temperature profiles at  $x/h = 3.75, 8.75$  (reacting flow, coarse grid):

\*\*\* Experiment, ••• LES (Colin-Algebraic, WD), ○○○ LES (Colin-Algebraic, JL), - - - LES (Charlette, JL), - · - · LES (Colin-Dynamic, JL)

The instantaneous and average temperature contours are shown in figure 10. A high average temperature region is also observed further downstream of the wake region, as also previously noted in [12]. This may be attributed to the roll-up of vortices downstream, enhancing the turbulence and wrinkling of the flame, thereby resulting in an increase of the flame surface and effective reaction rate, and producing intermittent fast local heat release.

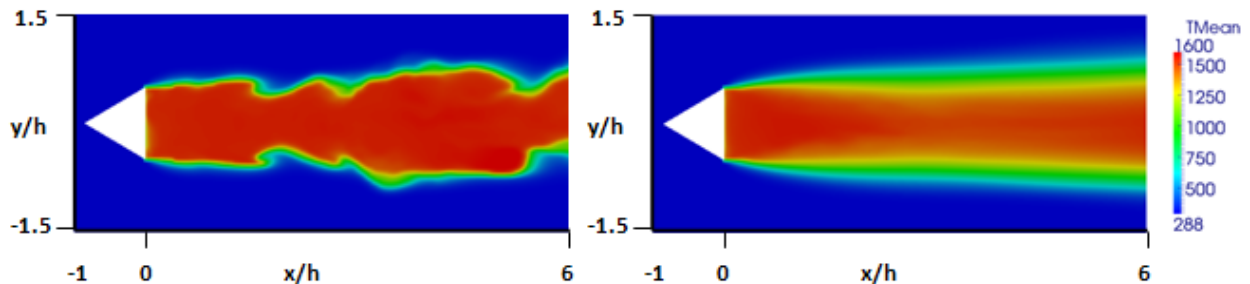


Figure 10: Temperature contours for reacting case: instantaneous temperature (left) and average temperature (right).

### C. Backward Facing Step Combustor: Non-Reacting Flow

Non-reacting flow is first simulated and the average and rms axial velocity profiles from simulations and experiments are compared at various cross sections downstream of the step. Simulation results show reasonable agreement with experimental measurements (figure 11) and the predicted reattachment length matches closely with the experimental observation ( $x/h=7.0$ ), although a slight under-prediction of the negative velocity is observed.

The velocity fluctuations are captured more accurately using the finer mesh, and although the shape of the profiles match the experimental observations for both cases, there is a marginal under-prediction of the velocity fluctuations in the shear layer region during the simulations.

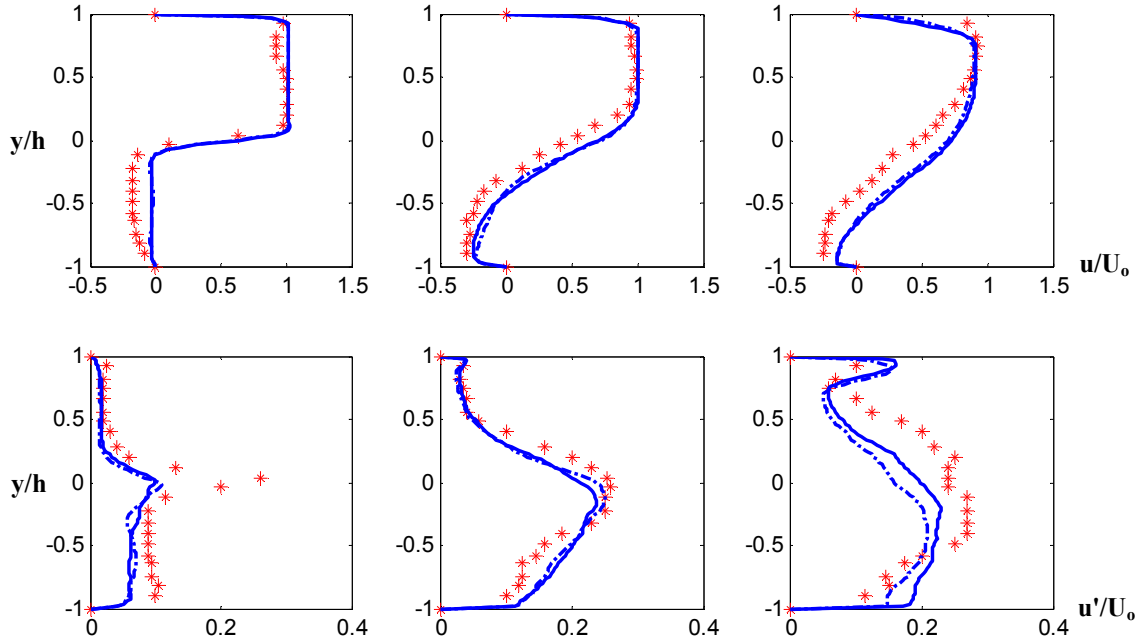


Figure 11: Normalized average/rms axial velocity profiles at  $x/H = 1, 3, 5$  (non-reacting flow):  
 \*\*\* Experiment, — LES (fine mesh), - - - LES (coarse mesh)

#### D. Backward Facing Step Combustor: Reacting Flow

Reacting flow simulations were performed next for the combustor using the thickened flame approach and different efficiency function models. A strong recirculation zone similar to the one present for the non-reacting case is noted for the reactive case, which however is shorter in this case (figure 12).

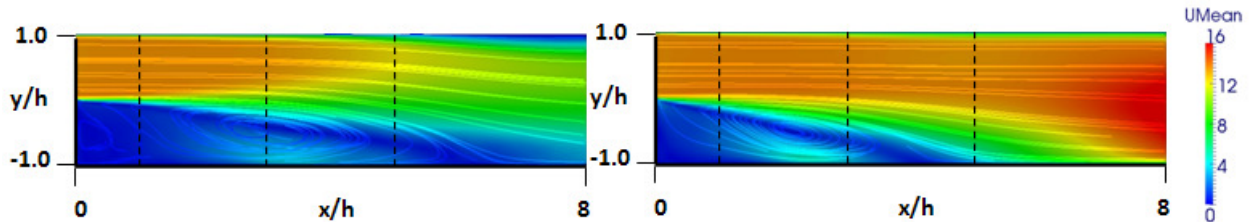


Figure 12: Average velocity magnitude contours and streamlines: non-reacting case (left), reacting case (right). The cross-sections at which data are compared are also shown.

In figure 13, the experimental data for the average axial velocity profiles measured at different cross sections along the combustor axis are shown and compared with the LES predictions obtained using the different efficiency function models. The results indicate reasonable agreement with experimental data for the average profiles, and the predicted reattachment length corresponds closely with the experimental value ( $x/h=4.5$ ), although a slight under-prediction of the negative velocity is observed in this case as well.

It is noted that the equation-based efficiency function formulation results in more accurate predictions (especially further downstream from the step) and captures the shear layer growth rate more effectively, while the single step reaction based simulations result in an over-estimation of the axial velocity magnitudes (due to inaccurate, higher temperature estimation). The maximum reverse velocity is also observed to be higher in this case, as compared to the non-reactive case, resulting from exothermicity and gaseous expansion.

The rms velocity profiles however differ markedly across the different cases, and while the shapes of the profiles match the experiments, there are varying degrees of over-prediction depending on the efficiency function model and reaction mechanism used. The single-step mechanism tends to significantly over-estimate the velocity fluctuations while the multiple-step reaction scheme predicts the velocity fluctuations with reasonable accuracy. It is also observed that the turbulence intensity reduces near the reattachment zone.

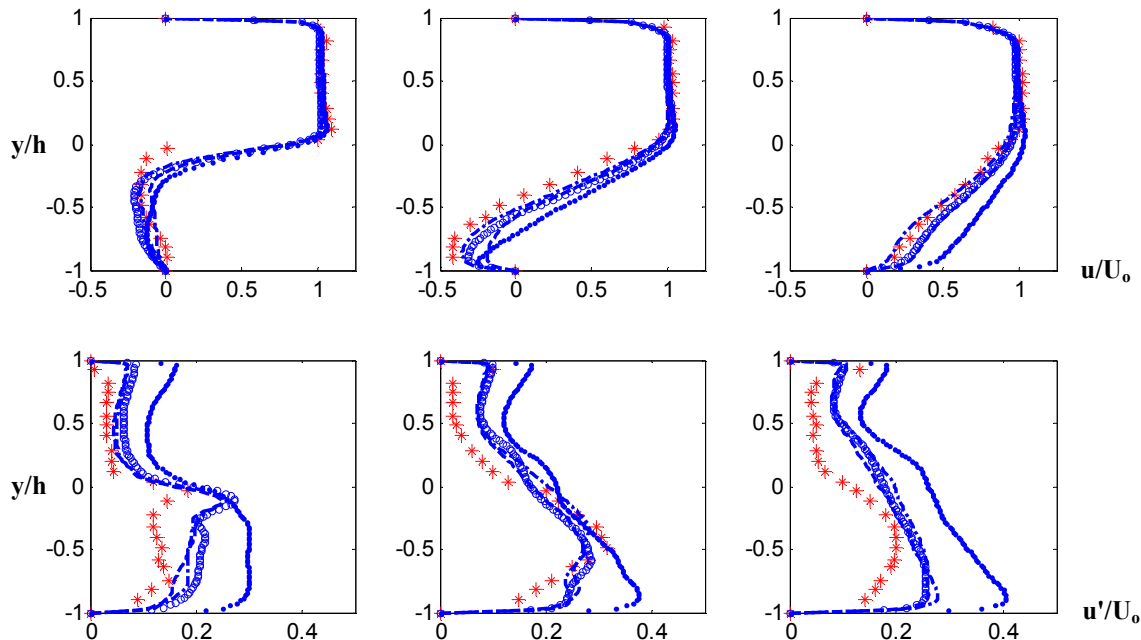


Figure 13: Normalized average/rms axial velocity profiles at  $x/H = 1, 3, 5$  (reacting flow, coarse grid):  
 \*\*\* Experiment, ●●● LES (Colin-Algebraic, WD), ○○○ LES (Colin-Algebraic, JL), - - - LES (Charlette, JL), - · - · LES (Colin-Dynamic, JL)

In figure 14, the experimental data for the average temperature profiles measured at different cross sections along the combustor axis are shown and compared with the LES predictions corresponding to the different efficiency function models. Again, the single-step mechanism over-predicts the temperature significantly, while the other cases perform more adequately, with the dynamic formulation resulting in more accurate estimations.

The steep gradient in the temperature profile ( $x/h < 1$ ) corresponds to the shear layer that gradually rolls up in a sequence of large-scale structures that grow downstream (as a result of entrainment, exothermicity, convective mixing and coalescence) and broaden the temperature profile. While this trend is captured by the combustion models, the spread of this high-turbulence region bounded by the shear layer (and consequently the progress of reaction) is slightly under-predicted in the simulations.

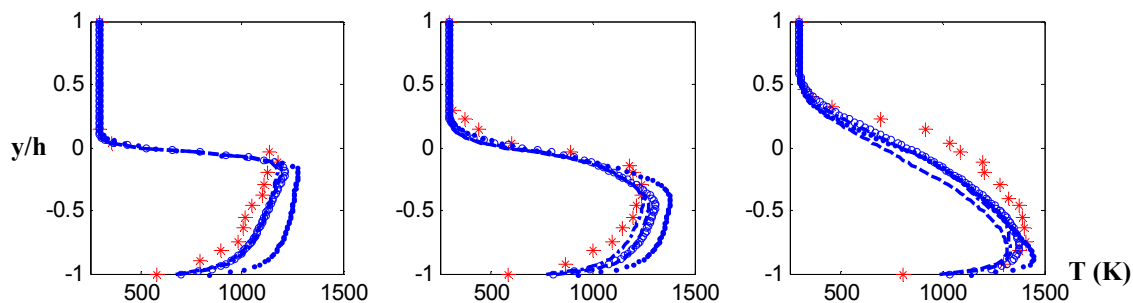


Figure 14: Average temperature profiles at  $x/H = 0.4, 1.2, 3.5$  (reacting flow, coarse grid):  
 \*\*\* Experiment, ●●● LES (Colin-Algebraic, WD), ○○○ LES (Colin-Algebraic, JL), - - - LES (Charlette, JL), - · - · LES (Colin-Dynamic, JL)

### E. Cylindrical Sudden Expansion Swirl Combustor: Non-Reacting Flow

Non-reacting flow is first studied and the average axial velocity profiles from simulations and experiments are compared at various cross sections downstream of the expansion plane of the cylindrical combustor. Simulation results show good agreement with experimental measurements when a fine mesh is used (figure 15) while the coarse mesh is unable to accurately capture the velocity flow-field in the recirculation zone region. As expected, a large central toroidal recirculation zone is found (figure 16) along with smaller vortices (actually vortex ring) at the corners of the chamber.

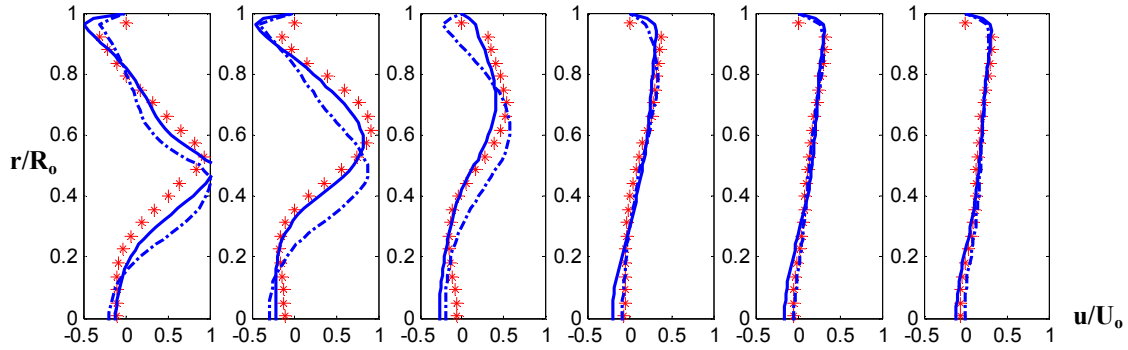


Figure 15: Normalized average axial velocity profiles at  $x/R_0 = 0.3, 0.6, 1.0, 1.4, 1.8, 2.2$  (non-reacting flow):  
 \*\*\* Experiment, — LES (fine mesh), - - - LES (coarse mesh)

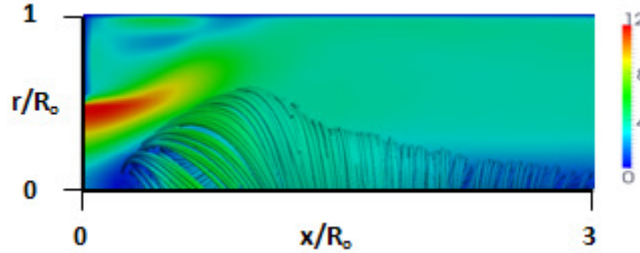


Figure 16: Average velocity contours and streamlines in central recirculation zone (non-reacting flow, fine mesh)

### F. Cylindrical Sudden Expansion Swirl Combustor: Reacting Flow

Reacting flow simulations are performed next for the combustor using the different efficiency function models. In figure 17, the experimental data for the average axial velocity profiles measured at different cross sections along the combustor axis is shown, and compared with LES predictions. Except the case with single-step reaction chemistry, each of the efficiency function models is able to capture the average velocity flow field reasonably accurately.

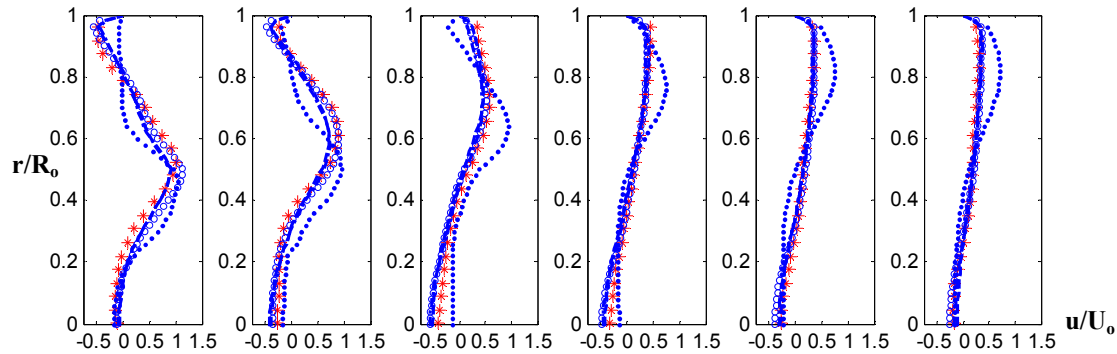


Figure 16: Normalized average axial velocity profiles at  $x/R_0 = 0.3, 0.6, 1.0, 1.4, 1.8, 2.2$  (reacting flow, fine grid):  
 \*\*\* Experiment, ••• LES (Colin-Algebraic, WD), ooo LES (Colin-Algebraic, JL), - - - LES (Charlette, JL), - · - · LES (Colin-Dynamic, JL)

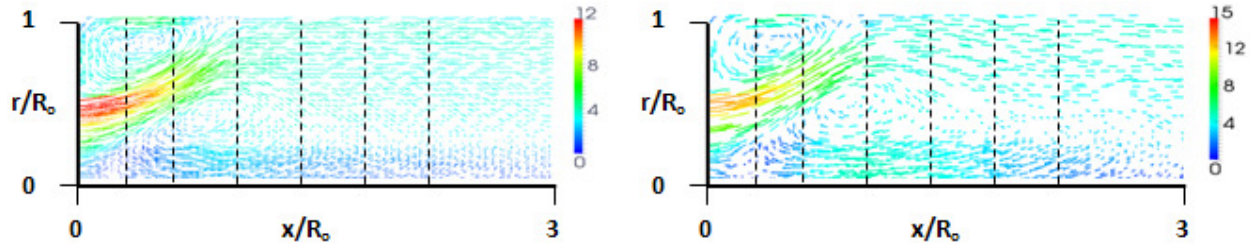


Figure 18: Average velocity 2D vector glyphs: non-reacting case (left), reacting case (right). The cross-sections at which data are compared are also shown.

## V. Conclusions

In this study, a preliminary analysis is conducted to assess the performance of turbulent-chemistry interaction sub-models on LES predictions for different combustor configurations. The simulation results are compared with experimental measurement, and the turbulent flow features are captured fairly well. More accurate predictions are obtained using a dynamic formulation for the efficiency function along with a multiple-step reaction mechanism.

## Acknowledgments

This research was funded under grant number KUS-110-010-01 from the King Abdullah University of Science and Technology. The contributions by Prof. Cheng Zhang and Dr. Neerav Abani are gratefully acknowledged.

## References

- [1] Ying H., Vigor Y., “Dynamics and stability of lean-premixed swirl-stabilized combustion,” *Progress in Energy and Combustion Science*, Vol. 35, Issue 4, pp. 293-364, 2009.
- [2] Garnier, E., Adams, N., and Sagaut, P., “Large eddy simulation for compressible flows”, Springer, 2009.
- [3] Echekki, T. “Turbulent combustion modeling: Advances, new trends and perspectives,” Springer-Verlag, 2011.
- [4] Roux, S., Lartigue, G., Poinso, T., Meier, U., and Bérat, C., “Studies of mean and unsteady flow in a swirled combustor using experiments, acoustic analysis, and large eddy simulations”, *Combustion and Flame*, Vol. 141, pp 40-54, 2005.
- [5] Colin, O., Ducros, F., Veynante, D., and Poinso, T., “A Thickened Flame Model for Large Eddy Simulation of Turbulent Premixed Combustion,” *Phys. Fluids*, Vol. 12, No. 7, pp. 1843–1863, 2000.
- [6] Charlette, F., Meneveau, C., and Veynante, D., “A Power-Law Flame Wrinkling Model for LES of Premixed Turbulent Combustion Part I: Non-Dynamic Formulation and Initial Tests,” *Combust. Flame*, Vol. 131, pp. 159–180, 2002.
- [7] Charlette, F., Meneveau, C., and Veynante, D., “A Power-Law Flame Wrinkling Model for LES of Premixed Turbulent Combustion Part II: Dynamic Formulation,” *Combust. Flame*, Vol. 131, pp. 181–197, 2002.
- [8] Weller, H.G., Tabor, G., Gosman, A.D., and Fureby C., “Application of a Flame Wrinkling LES Combustion Model to a Turbulent Mixing Layer”, 27<sup>th</sup> Symposium on Combustion, The Combustion Institute, pp. 899-907, 1998.
- [9] Selle, L., Lartigue, G., Poinso, T., Kaufmann, P., Krebs, W., and Veynante, D., “Large Eddy Simulation of Turbulent Combustion for Gas Turbines with Reduced Chemistry”, *Proc. of Summer Program 2002*, Center for Turbulence Research.
- [10] Durand, L., and Polifke, W., “Implementation of the Thickened Flame Model for Large Eddy Simulation of Turbulent Premixed Combustion in a Commercial Solver,” *ASME Paper No. GT2007-28188*, 2007.
- [11] Polifke, W., Hirsch, C., Zellhuber, M., Komarek, T., and Chong, L., “Influence of strain and heat loss on flame stabilization in a non-adiabatic combustor”, *Proceedings of the European Combustion Meeting*, 2009.
- [12] Giacomazzi, E., Battaglia, V., and Bruno, C., “The Coupling of Turbulence and Chemistry in a Premixed Bluff Body Flame as Studied by LES”. *Combustion and Flame*, Vol. 138, pp. 320-335, 2004.
- [13] Jones, W.P., and Lindstedt, R.P., “Global reaction schemes for hydrocarbon combustion,” *Combustion and Flame*, Vol. 73, Issue 3, pp. 233-249, 1988.
- [14] C. Fureby, C. Löfström, Large-eddy simulations of bluff body stabilized flames, *Symposium (International) on Combustion*, Volume 25, Issue 1, 1994, Pages 1257-1264.
- [15] Pitz, R.W., and Daily, J.W., “Combustion in a Turbulent Mixing Layer Formed at a Rearward Facing Step”, *AIAA Journal*, Vol. 21, Issue 11, pp. 1565-1570, 1983.
- [16] Speth, R., Altay, H., Hudgins, D., Annaswamy, A., and Ghoniem, A. “Vortex-Driven Combustion Instabilities in Step and Swirl-Stabilized Combustors”, in the 46th AIAA Aerospace Sciences Meeting, Reno, NV, January 2008.
- [17] LaBry, Z., Shanbhogue, S., Speth, R., and Ghoniem, A., “Flow structures in a lean-premixed swirl-stabilized combustor with microjet air injection”, *Proceedings of the Combustion Institute*, Vol. 33, pp 1575-1581, 2011.